physica status solidi pss a
www.pss-a.com

Surface Plasmon Enhanced Emission From Defects in Gallium Doped ZnO

Yaonan Hou, Zengxia Mei,* Aihua Tang, Huili Liang, and Xiaolong Du**

In this work, the optical properties of defects coupled with surface plasmons (SPs) in gallium-doped ZnO (ZnO:Ga) grown by molecular beam epitaxy (MBE) have been explored. The photoluminescence intensity is enhanced by up to 4.9 times as a result of SPs coupling by decorating the sample with silver nanospheres (Ag NSs), with a fast plasmonic decay lifetime of 0.1 ns compared with the defect-assisted carrier recombination lifetime of 3.77 ns in the as-grown sample. The enhanced emission intensity depends on the plasmonic modes determined by the diameter of Ag NSs, verified by power-dependent photoluminescence measurements. Confocal mapping reveals that the plasmonic "hot-spots", that is, enhanced emission around the Ag NSs, exhibit a highly optical stability with reduced photoluminescence blinking. This work demonstrates that a defect coupled with SPs in ZnO is a promising high-efficiency emitter for applications in nanophotonics.

1. Introduction

ZnO has been regarded as a promising candidate for optoelectronic and photonic applications thanks to its unique optical properties, such as the direct wide band gap of 3.37 eV along with a large exciton binding energy of 60 meV.[1,2] In spite of this, optical dynamics of defect-related emission from ZnO in visible region has been a long-term controversy compared with its ultraviolet band edge emission.[3] Generally speaking, for example, the green-yellow band emission is considered to be related with oxygen vacancies (V_O)[4,5]; blue-violet emission attributed to Zn interstitials (Zn_i) and Zn vacancies (V_{Zn})[5–7]; and orange-red emission assigned to the oxygen interstitials (O_i) or charged V_O.[8,9] Electron transitions between the energy levels of such intrinsic point defects and the conduction/valence band minimum/maximum (CBM and VBM) are rather complicated. In addition to such intrinsic point defects, the defects introduced by doping the host ZnO with foreign atoms are a key factor to determine its electrical and optical properties. Compared with the effort made in the research on the electrical properties of doped ZnO, less attention has been paid to the optical dynamics and the potential optical applications of an extrinsic defect, especially for the defect complex which is potentially a new single photon source in analogy to the nitrogen-vacancy center in diamond.[10] Identification and manipulation of the defect-related emission in ZnO are crucial to realize novel optoelectronic/photonic devices, such as full color light-emitting devices and single photon sources.[11–15] Furthermore, exotic optical properties can be obtained by control the defect density, as demonstrate in the recent progresses in gallium-doped ZnO (ZnO:Ga).[16,17]

Surface plasmon (SP) is a collective oscillation of surface electrons in a metal which is placed in vicinity of a dielectric material under the excitation of light. Considering the large momentum of SPs due to the participation of electrons, a high optical density of states (DoS) is expected. The radiation rate (r) will be enhanced according to Fermi's Golden rule, $r \propto |\langle m|\vec{p}\vec{E}|n\rangle|^2 \rho(\hbar\omega)$, where $\langle m|\vec{p}\vec{E}|n\rangle$ is dipole emission matrix element and $\rho(\hbar\omega)$ the optical DoS. Moreover, the energy of the defect dipole can directly transfer to the SPs such that the "dark" defect will be ignited,[18] further enhancing the emission. In term of this, a number of SPs enhanced emitters have been developed, especially the defect related emitters.[19,20] For the same reason, SPs enhanced emission is also applicable to the defect related emission in ZnO,[21–23] which enables the development of novel photonic devices to manipulate light-matter interactions based on ZnO.

In this work, we studied the defect coupled with plasmonic modes by optical excitation of silver (Ag) nanospheres decorated ZnO:Ga (Ag NSs/ZnO:Ga) thin film. By changing the diameter of Ag NSs, different plasmonic modes were observed from theoretical simulation and optical characterizations. The photoluminescence (PL) intensity increases by up to 4.9 folds compared with that from as grown ZnO:Ga, with the diameter of Ag NSs ranging from 20 to 40 nm. The dynamics of electron transition in these defects coupled with SPs modes are investigated by time-resolved photoluminescence (TRPL), which shows a fast SPs decay lifetime down to 0.1 ns in presence of Ag NSs compared with the recombination lifetime of 3.77 ns in as grown sample. The optical properties are further studied by power-dependent photoluminescence (PDPL) measurements, showing enhanced emission intensity sublinearly depends on the excitation power density and the plasmonic modes. Confocal PL reveals that the hot spots where

Dr. Y. Hou, Prof. Z. Mei, A. Tang, Dr. H. Liang, Prof. X. Du
Beijing National Laboratory for Condensed Matter Physics
Institute of Physics
Chinese Academy of Sciences
Beijing 100190, China
E-mail: houyaonan@gmail.com; zxmei@iphy.ac.cn; xldu@iphy.ac.cn
Prof. X. Du
School of Physical Sciences
University of Chinese Academy of Sciences
Beijing 100190, China

DOI: 10.1002/pssa.201800037

SPs enhanced emission is observed exhibit an excellent reliability without blinking, as is observed from the defect emission in as-grown sample. Our results demonstrate that defect–SPs coupling in ZnO is an efficient system promisingly useful for photonic devices.

2. Experimental Section

Our ZnO:Ga sample was grown by radio frequency plasma assisted molecular beam epitaxy (rf-MBE) equipped with an in-situ reflection high-energy electron diffraction (RHEED) to monitor the whole growth process. The growth temperature and thickness of the sample were 600 °C and 350 nm, respectively. The carrier concentration and mobility were $\approx 9 \times 10^{17}\,\mathrm{cm}^{-3}$ and 17 cm/(V·s) according to room temperature Hall measurements. More details about the growth can be found elsewhere.[24]

The Ag NSs/ZnO:Ga structure was fabricated by drop-casting Ag NSs (Sigma–Aldrich) with diameters of 20, 30, and 40 nm directly on the surface of our sample. Reflectance measurement was performed using a 75 W Xe lamp followed with a 0.5 m monochromator (Acton Research Corporation, SpectraPro-500i), whilst the intensity was recorded by a Si enhanced photodetector. Room temperature PL and TRPL was performed by a micro-PL (μ-PL) system with excitation of a 375 nm pulsed laser. The beam was focused into a spot of ≈2 μm in diameter on the sample with a 50× objective lens. The emission light was coupled to a monochromator (Acton Research Corporation, HRS-300) with a photomultiplier tube. PDPL was performed in the same system but with a 375 nm continuous wave laser, and a thermoelectric cooled charge-coupled device (CCD). PL mapping was carried out using a commercial confocal system (WiTec 300R) with a 100× objective length to focus the laser beam down to ≈300 nm. The laser power was about 1 mW, measured before being coupled into the confocal system. All the optical experiments were performed at room temperature.

3. Results and Discussion

Figure 1a schematically shows the configuration of our sample, where Ag NSs are placed on ZnO:Ga. Plasmonic coupling is expected if any defect locating underneath the Ag NSs is within the electric field penetration depth of SPs. Figure 1b–d display the scanning electron microscopy (SEM) images of the samples with NS diameters of 20, 30, and 40 nm, respectively. Some of NSs are marked in the images to better visualize their positions. Because the NSs are transferred on to our sample by drop-casting method, they are randomly distributed on the surface. The sample with 20 nm NPs has the highest density of $\approx 1 \times 10^{11}\,\mathrm{cm}^{-2}$; and the other two are $3 \times 10^{9}\,\mathrm{cm}^{-2}$ (30 nm NS) and $2 \times 10^{9}\,\mathrm{cm}^{-2}$ (40 nm NS), respectively. Compared with previous work using Ag nanoislands formed in a self-organization process by deposition and post-annealing approach,[23] the shape and size are deterministic. Therefore, the SPs mode is more easily to be controlled.

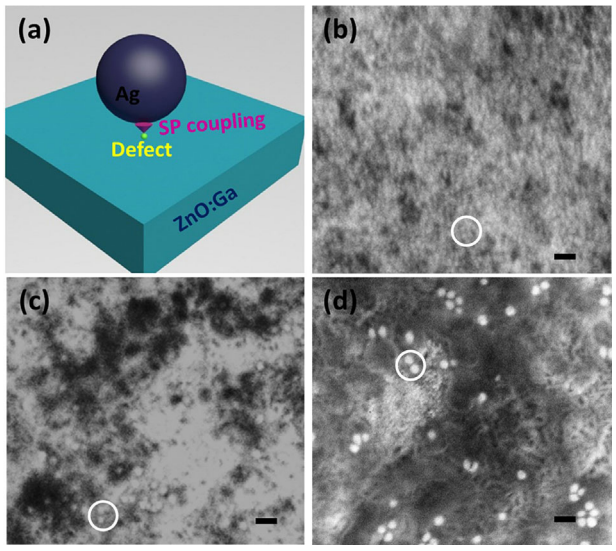

Figure 1. a) Schematic of the sample structure, comprising of a Ag NS placed on the surface of ZnO:Ga. b–d) SEM images of ZnO:Ga decorated with Ag NSs with diameter of 20, 30, and 40 nm, respectively (scale bar = 100 nm). The positions of Ag NSs is partly marked in the images.

In order to have a first impression of the defect-SPs coupling in Ag NSs/ZnO:Ga structure, we initially perform finite-difference time-domain (FDTD) simulation, with a randomly polarized excitation light source (total-field scattering-field souce), with the emission wavelength from 450 to 750 nm. The refractive index of

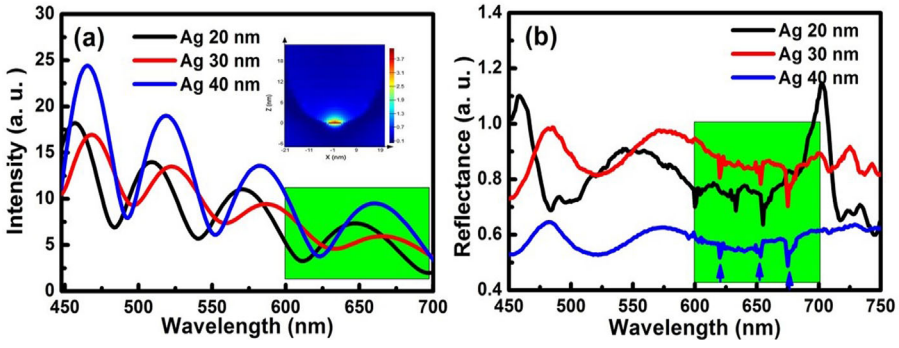

Figure 2. a) FDTD simulated emission spectra of ZnO:Ga with Ag NSs; inset shows the mode profile of 40 nm Ag NSs on ZnO:Ga. b) Reflectance of the samples with Ag NSs with respect to the as grown sample.

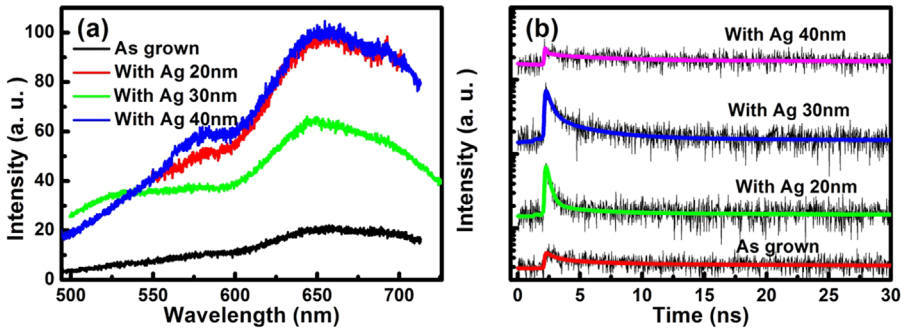

Figure 3. a) Room-temperature μ-PL spectra of all the samples. b) Time-resolved μ-PL decay traces of all the samples; the thick color lines are the fitting curves.

Table 1. The fitting results of the time-resolved PL decay traces by Eqs. (1) and (2).

Sample	τ_{sp} (ns)	τ_1(ns)	τ_2 (ns)
As grown		3.77	28.1
20 nm	0.329	2.86	35.0
30 nm	0.446	3.33	39.4
40 nm	0.10	1.52	31.2

ZnO and Ag are set to 2 and Johnson and Christy values, respectively.[25] The emission spectra are obtained by suing a time-monitor. **Figure 2**a shows the SPs emission spectra which are clearly related with the diameter. The region with wavelengths ranging from 600 to 750 nm (marked area in Figure 2a) is most interesting to us because it corresponds to the defect emission of our ZnO:Ga sample (**Figure 3**a). The strongest emission is from the sample with 40 nm Ag NSs, and the weakest is from the 30 nm Ag NSs with a peak around 650 nm. The inset of Figure 2a shows the mode profile of SPs in a 40 nm Ag NS, where a strong localized electric field distributed near the Ag/ZnO:Ga interface can be seen. Reflectance measurment is performed to further verify the existence of SPs. As shown in Figure 2b, the reflectance with arbitrary unit is obtained by dividing the reflected light intensity of the sample with Ag NSs by the one of as-grown sample. Valleys with minimum value at ≈650 nm for all the three samples are due to SPs enhanced absorption, agreeing well with the simulation results. In addition, some fine structures with full width at half maximum (FWHM) of ≈5 nm are observed (labeled in Figure 2b), with an unclear origin. We would like to attribute them to SPs cavity modes formed between adjacent Ag NSs, as the line width is similar to the reported value of a plasmonic nanocavity.[26,27]

Room-temperature μ-PL spectra of all the samples are shown in Figure 3a. Due to the presence of Ag NSs, the broad red emission

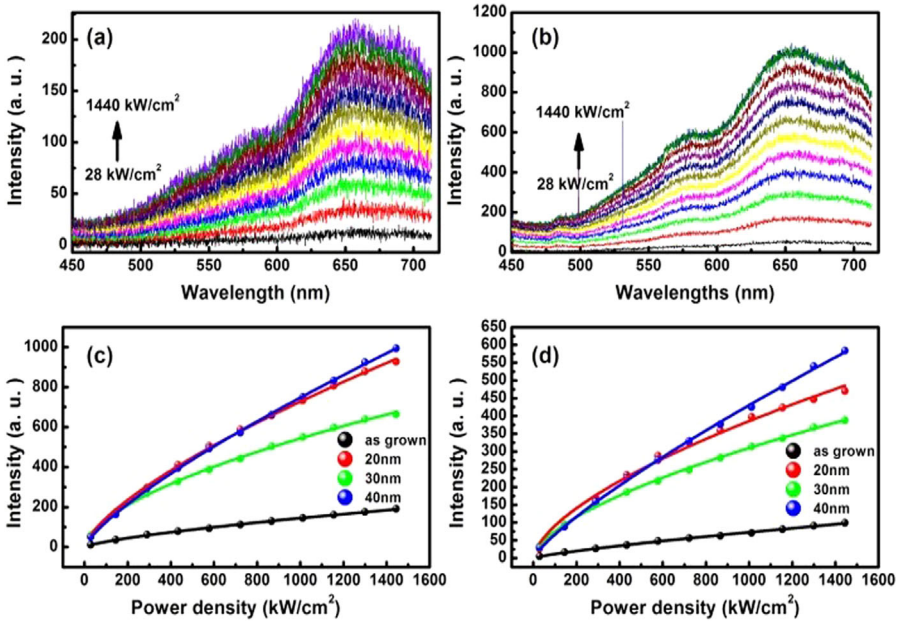

Figure 4. Power-dependent μ-PL spectra of the as grown sample (a) and the sample with 40 nm Ag NSs (b); and the emission intensity plotted against excitation power density of the samples for the main peak (c) and the shoulder (d).

Table 2. The fitting parameters of the power-dependent PL measurements.

Sample	β_1(main)	β_1(shoulder)
As grown	0.73	0.80
20 nm	0.70	0.63
30 nm	0.60	0.61
40 nm	0.77	0.81

with a peak at 650 ± 5 nm is greatly enhanced. The enhancement factors are 4.8, 3.2, and 4.9 for the samples with 20, 30, and 40 nm Ag NSs, respectively. Apart from the main peak, a shoulder of yellow emission at 575 nm also becomes noticeable. It is worth to mention that the emission could be quenched due to the coupling to nonradiative plasmonic modes if the distance between the defect and Ag NSs is less than ≈5 nm.[28] Compared with the penetration depth of SPs in ZnO (≈180 nm at 650 nm), the number of quenched defects is very limited in our situation. As a result, only PL enhancement is observed. To corroborate the enhanced emission resulting from SPs coupling instead of scattering, TRPL is performed at room temperature with the μ-PL system shown in Figure 3b, where a lower intensity of the sample with 40 nm Ag NSs compared with the other two is due to a filter added for the emission collection. For the as grown sample, the decay trace is fitted to biexponential decay,[29]

$$I(t) = a_1 \exp(-\frac{t}{\tau_1}) + a_2 \exp(-\frac{t}{\tau_2}) \quad (1)$$

where a_1 and a_2 are the fitting parameters; τ_1 and τ_2 are the fast and slow decay components. τ_1 is regarded as the PL decay time (τ_{pl}) related with radiative recombination via the defect, and τ_2 related with the nonradiative processes. With the SPs coupling, a third term is introduced,

$$I(t) = a_1 \exp(-\frac{t}{\tau_1}) + a_2 \exp(-\frac{t}{\tau_2}) + a_3 \exp(-\frac{t}{\tau_{sp}}) \quad (2)$$

where τ_{sp} is the decay lifetime related with SPs modes, and a_3 the additional fitting parameter. Equations (1) and (2) are well-fitted with our results shown in Figure 3b. The decay lifetimes are shown in **Table 1**, where τ_{sp} is 0.329, 0.446, and 0.1 ns for 20, 30, and 40 nm Ag NSs, respectively. The shortest decay lifetime indicates the best defect-coupling in the sample with 40 nm Ag NSs, agreeing well with the FDTD simulations and reflectance measurements (Figure 2). Note τ_{sp} is clearly much shorter than τ_1 and τ_2. Supposing the light out-coupling from SP modes is unit, the quantum efficiency of the plasmonic emission is,

$$\eta = \frac{\frac{1}{\tau_{sp}}}{\frac{1}{\tau_{sp}} + \frac{1}{\tau_1} + \frac{1}{\tau_2}} \times 100\% \quad (3)$$

where η is the quantum efficiency, and $\frac{1}{\tau_i}(i = 1, 2, sp)$ the decay rate corresponding to the three terms in Eq. (2). Since $\frac{1}{\tau_{sp}} \gg \frac{1}{\tau_t}, \frac{1}{\tau_2}$, according to the fitting results, η can approach 100%, indicating the defects coupled with the SPs a superior light emitter. In practice, plasmonic emission is influenced by the out-coupling efficiency and dipole-SPs coupling efficiency, which often leads to a definite enhancement. It is known that the coupling wavelength and strength strongly depend on the geometry and dimensions of the metal nanostructure on a flat semiconductor material.[23,30] In our case, only the diameters are tuned to

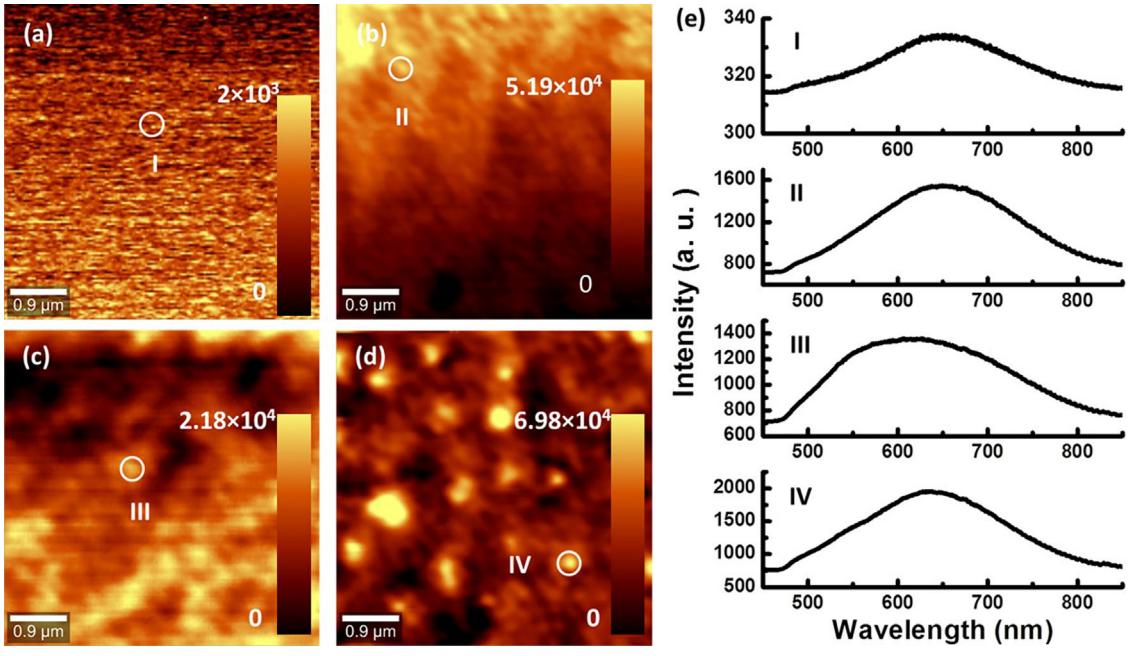

Figure 5. Confocal PL mapping of the as grown sample (a), the sample with 20 nm Ag NSs (b), the sample with 30 nm Ag NSs (c), the sample with 40 nm Ag NSs (d); and (e) the emission spectra corresponding to the hot spot (I), (II), (III), and (IV) in the labeled sites.

enhance the coupling between SPs mode and the defect in ZnO:Ga. Therefore, it is reasonably to attribute the best coupling of 40 nm Ag NSs to its size.

The defect-SPs coupling is further studied by PDPL with the pumping power density increased from 28 to 1440 kW cm^{-2}. **Figure 4**a and b display the PDPL spectra of the as grown and the sample with 40 nm NSs measured under identical conditions. In addition to the main peak at ≈650 nm, the shoulder emission at 575 nm is also enhanced. Figure 4c and d are the plots of emission intensity as a function of optical pumping power density, which can be fitted to the relationship of $I \propto P^{\beta}$, with fitting results shown in **Table 2**, where I and P are the emission and pumping intensities, respectively. The exponent β is related with the carrier recombination and energy transfer process.[31] For the as grown sample, $\beta = 0.73$ (0.80) is obtained for the main peak (shoulder peak), which is increased to 0.77 (0.81) by introducing 40 nm NSs. The results suggest the radiative recombination is greatly improved with SPs coupling. In contrast, β values of the samples with 20 and 30 nm Ag NSs are 0.7 (0.63) and 0.6 (0.61), which are smaller than that of as grown sample. The decreased β value with the increasing pumping power density indicates quantum efficiency drooping due to the mode shifting, leading the energy partly coupled to dark modes. This is also seen from the differences in the lifetimes of SPs emissions in the three samples (Table 1). However, the overall emission intensity is still enhanced due to the participation of additional number of nonradiative defects. As defects in semiconductor may act as nonraditive centers, where the energy generated from electron-hole recombination is passed to the lattice vibration. When such defects are coupled with SPs, the energy is transferred into plamsonic modes owing to the strongly localized field. As a result, the emission intensity is still enhanced for the samples with 20 and 30 nm Ag NSs.

Confocal PL characterizations are carried out with a scanning area of 5 × 5 μm^2. **Figure 5**a shows the scanning image of the as grown ZnO:Ga, where discrete bright spots can be observed, reflecting the distribution of the radiative defects (or defect clusters) in our sample. It is worth to mention that we cannot rule out the emission from a single defect, which needs further inspection by second order correlation measurements as reported in previous work.[13–15] For the samples with Ag NSs (Figure 5b–d), strong localized emission around the Ag NSs can be observed as a result of SPs enhancement, often referred to as "hot spots".[32,33] Selected emission from single Ag NSs from the

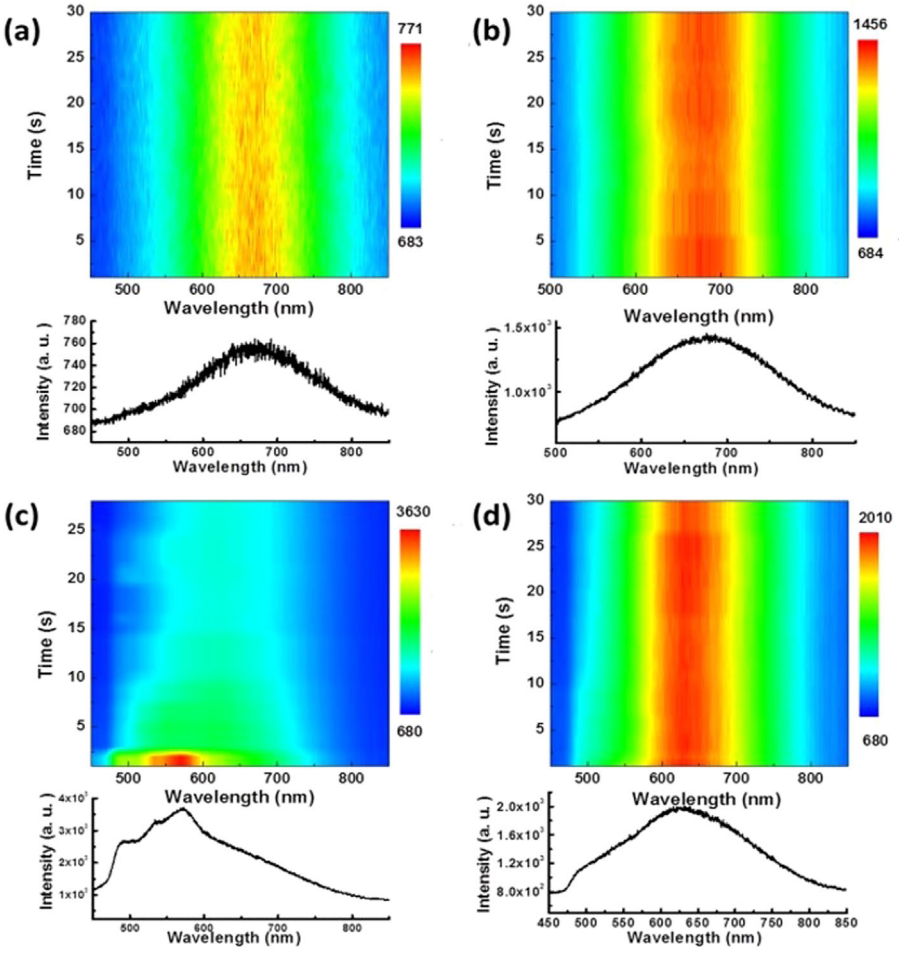

Figure 6. Contour plots of PL intensity as a function of time and wavelengths of the as grown sample (a), ZnO:Ga with 20 nm Ag NSs (b), ZnO:Ga with 30 nm Ag NSs (c), and ZnO:Ga with 40 nm Ag NSs (d).

four samples denoted as I, II, III, and IV are shown in Figure 4e. The highest enhancement is the sample with 40 nm Ag NSs, agreeing well with TRPL measurements. In addition, the strength of localized electric field decreases quickly in both materials due to its evanescent nature. Therefore, defect-SPs coupling strength depends on the depth of the defects locating within the penetration depth of SPs, which leads to the variation of emission density between different NSs in the same sample, as observed from the confocal scanning.

Optical stability of defect emission is another key parameter which determines the reliability of a practical device. Previous work on ZnO single defect emissions observed strong blinking and spectral jumping due to a fluctuation of the electrostatic environment surrounding the defect.[13,15] In order to investigate the optical stability, we have continuously captured the emission spectrum every one second. **Figure 6a–d** exhibit the contour plots of the emission intensity as a function of the time and wavelength. To be clear, the emission spectrum at the first second is also provided under each plot. A clear blinking is observed from the as grown sample (Figure 6a) in contrast to the stable emission from the samples with 20 and 40 nm NSs (Figure 6b and d). This phenomenon indicates the coupled defect-SPs system is not vulnerable to the electrostatic environment, enhancing the stability of the emitter. Similar results in the SPs enhanced band edge emission in ZnO have also been reported.[34] Figure 6c shows the emission from a cluster of 30 nm NSs on ZnO:Ga. The emission spectrum exhibits three clear plasmonic modes with wavelengths shorter than 600 nm at the first second, distinguishing from Figure 6a and Figure 5e(III) due to the cluster size. The peak continuously shifts towards 650 nm and eventually becomes similar with the one shown in Figure 5e(III) as a result of heating under the cw excitation of $\approx 1.4\,\mathrm{MW\,cm^{-2}}$, which causes the separation of the cluster.

4. Conclusion

In conclusion, defect–SPs coupling has been systematically studied in Ag NSs/ZnO:Ga structure with different NS diameters. The existence of plasmonic modes is initially confirmed with FDTD simulation and reflectance measurement. From integral micro-PL measurements, high emission intensity is observed with the enhancement factors up to 4.9 due to the rapid recombination induced by defect–SPs coupling, which is corroborated by TRPL measurements. From PDPL characterization, it is found that the emission intensity is closely related with the plasmonic modes. The hot spots strongly localized at the NSs sites are observed from the confocal mapping. They further confirm the defect–SPs coupling, which demonstrates an excellent optical stability with reduced PL blinking, promising for the application in single photon sources.

Acknowledgement

This work was supported by the National Natural Science Foundation of China (Grants No. 11674405, 11675280, 11274366, 51272280, and 61306011).

Conflict of Interest

The authors declare no competing financial interest.

Keywords

defects, doping, photoluminescence, surface plasmons, ZnO

Received: January 17, 2018
Revised: February 8, 2018
Published online:

[1] T. Makino, C. H. Chia, N. T. Tuan, Y. Segawa, M. Kawasaki, A. Ohtomo, K. Tamura, H. Koinuma, *Appl. Phys. Lett.* **2000**, *76*, 3549.
[2] D. C. Reynolds, D. C. Look, B. Jogai, C. W. Litton, G. Cantwell, W. C. Harsch, *Phys. Rev. B* **1999**, *60*, 2340.
[3] A. Janotti, C. G. Van de Wall, *Phys. Rev. B* **2007**, *76*, 165202.
[4] J. D. Ye, S. L. Gu, F. Qin, S. M. Zhu, S. M. Liu, X. Zhou, W. Liu, L. Q. Hu, R. Zhang, Y. Shi, Y. D. Zheng, *Appl. Phys. A* **2005**, *81*, 759.
[5] C. H. Ahn, Y. Y. Kim, D. C. Kim, S. K. Mohanta, H. K. Cho, *J. Appl. Phys.* **2009**, *105*, 013502.
[6] S. H. Jeong, B. S. Kim, B. T. Lee, *Appl. Phys. Lett.* **2003**, *82*, 2625.
[7] H. Zeng, G. Duan, Y. Li, S. Yang, X. Xu, W. Cai, *Adv. Funct. Mater.* **2010**, *20*, 561.
[8] N. H. Alvi, K. Ul Hasan, O. Nur, M. Willand, *Nanoscale Res. Lett.* **2011**, *6*, 130.
[9] K. Bandopadhyay, J. Mitra, *RSC Adv.* **2015**, *5*, 23540.
[10] I. Aharonovich, D. Englund, M. Toth, *Nat. Photonics* **2016**, *10*, 631.
[11] S. Vempati, J. Mitra, P. Dawson, *Nanoscale Res. Lett.* **2012**, *7*, 470.
[12] P. Chen, X. Ma, Y. Zhang, D. Li, D. Yang, *J. Electron Mater.* **2010**, *39*, 652.
[13] O. Neitzke, A. Morfa, J. Wolters, A. W. Schell, G. Kewes, O. Benson, *Nano Lett.* **2015**, *15*, 3024.
[14] N. R. Jungwirth, H.-S. Chang, M. Jiang, G. D. Fuchs, *ACS Nano* **2016**, *10*, 1210.
[15] A. J. Morfa, B. C. Gibson, M. Karg, T. J. Karle, A. D. Greentree, P. Mulvaney, S. Tomljenovic-Hanic, *Nano Lett.* **2012**, *12*, 949.
[16] S. Kalusniak, S. Sadofev, F. Henneberger, *Phys. Rev. Lett.* **2014**, *112*, 137041.
[17] T. Tyborski, S. Kalusniak, S. Sadofev, F. Henneberger, M. Woerner, T. Elsaesser, *Phys. Rev. Lett.* **2015**, *115*, 147401.
[18] T. Ozel, P. L. Hernandez-Martinez, E. Mutlugun, O. Akin, S. Nizamoglu, I. O. Oze, Q. Zhang, Q. Xiong, H. V. Demir, *Nano Lett.* **2013**, *13*, 3065.
[19] A. Huck, S. Kumar, A. Shakoor, U. L. Andersen, *Phys. Rev. Lett.* **2011**, *106*, 096801.
[20] S. Kumar, A. Huck, U. I. Andersen, *Nano Lett.* **2013**, *13*, 1221.
[21] B. J. Lawrie, R. Mu, R. F. Haglund, *Opt. Lett.* **2012**, *37*, 1538.
[22] T. N. Xu, L. Hu, S. Q. Jin, B. P. Zhang, X. K. Cai, H. Z. Wu, C. H. Sui, *Appl. Surf. Sci.* **2012**, *258*, 5886.
[23] T. Nakamura, *Phys. Rev. Appl.* **2016**, *6*, 044009.
[24] A. Tang, Z. Mei, Y. Hou, L. Liu, V. Venkatachalapathy, A. Azarov, A. Kuznetsov, X. Du, **2017**, arXiv:1709.07603.
[25] P. B. Johnson, R. W. Christy, *Phys. Rev. B* **1972**, *6*, 4370.
[26] Y. J. Lu, J. Kim, H. Y. Chen, C. Wu, N. Dabidian, C. E. Sanders, C. Y. Wang, M. Y. Lu, B. H. Li, X. Qiu, W. H. Chang, L. J. Chen, G. Shvets, C. K. Shih, S. Gwo, *Science* **2012**, *337*, 450.
[27] Y. J. Lu, C. Y. Wang, J. Kim, H. Y. Chen, M. Y. Lu, Y. C. Chen, W. H. Chang, L. J. Chen, M. I. Stockman, C. K. Shih, S. Gwo, *Nano Lett.* **2014**, *14*, 4381.

[28] M. Liu, R. Chen, G. Adamo, K. F. MacDonald, E. J. Sie, T. C. Sum, N. I. Zheludev, H. Sun, H. J. Fan, *Nanophotonics* **2013**, *2*, 153.
[29] K. Okamoto, I. Niki, A. Scherer, Y. Narukawa, T. Mukai, Y. Kawakami, *Appl. Phys. Lett.* **2005**, *87*, 071102.
[30] X. Xu, M. Funato, Y. Kawakami, K. Okamoto, K. Tamada, *Opt. Express* **2013**, *21*, 3145.
[31] M. Saba, M. Cadelano, D. Marongiu, F. Chen, V. Sarritzu, N. Sestu, C. Figus, M. Aresti, R. Piras, A. G. Lehmann, C. Cannas, A. Musinu, F. Quochi, A. Mura, G. Bongiovanni, *Nat. Commun.* **2014**, *5*, 5049.
[32] B. Lahiri, G. Holland, V. Aksyuk, A. Centrone, *Nano Lett.* **2013**, *13*, 3218.
[33] C. T. Ersgaard, R. M. McKoskey, I. S. Rich, N. C. Lindquist, *ACS Nano* **2014**, *8*, 10941.
[34] H. Shen, C. X. Shan, Q. Qiao, J. S. Liu, B. H. Li, D. Z. Shen, *J. Mater. Chem. C* **2013**, *1*, 134.